



# A two-point correlation function for Galactic halo stars

A. P. Cooper,<sup>1,2</sup> S. Cole,<sup>1</sup> C. S. Frenk<sup>1</sup> and A. Helmi<sup>3</sup>

<sup>1</sup>Institute for Computational Cosmology, Department of Physics, University of Durham, South Road, Durham DH1 3LE

<sup>2</sup>Max-Planck-Institut für Astrophysik, Karl-Schwarzschild-Str. 1, D-85748 Garching, Germany

<sup>3</sup>Kapteyn Astronomical Institute, University of Groningen, PO Box 800, 9700 AV Groningen, the Netherlands

Accepted 2011 July 7. Received 2011 July 6; in original form 2010 November 9

## ABSTRACT

We describe a correlation function statistic that quantifies the amount of spatial and kinematic substructure in the stellar halo. We test this statistic using model stellar halo realizations constructed from the Aquarius suite of six high-resolution cosmological  $N$ -body simulations, in combination with the GALFORM semi-analytic galaxy formation model. The stellar haloes in these simulations, which form from disrupted satellites accreted between redshifts 1 and 7, show considerable scatter in the nature of their substructure. We find that our statistic can distinguish between these different realizations of plausible models for the global structure of the Milky Way stellar halo. We apply our statistic to a catalogue of blue horizontal branch stars identified in the Sloan Digital Sky Survey. In our  $\Lambda$  cold dark matter simulations, we find examples of haloes with spatial and kinematic substructure consistent with the available Milky Way data in the outer halo. For the inner halo, the models predict stronger clustering than observed, suggesting the existence of a smooth component, not currently included in our simulations.

**Key words:** methods: numerical – Galaxy: halo – Galaxy: structure – galaxies: haloes.

## 1 INTRODUCTION

In the cold dark matter (CDM) cosmogony, galactic stellar haloes are built up in large part from the debris of tidally disrupted satellites (e.g. Searle & Zinn 1978; White & Springel 2000; Bullock & Johnston 2005; Cooper et al. 2010). Discovering and quantifying halo structures around the Milky Way (MW) may provide a useful diagnostic of the Galaxy’s merger history (e.g. Helmi & de Zeeuw 2000; Johnston et al. 2008; Gómez & Helmi 2010). Upcoming MW surveys (for example with the PanSTARRS1, LAMOST, HERMES and LSST) will provide large data sets in which to search for structure. The *Gaia* mission will determine six-dimensional phase-space coordinates for all stars brighter than  $V \sim 17$ , from which it should be possible to untangle even well-mixed streams in the nearby halo (Gómez et al. 2010).

Testing the CDM model by comparing these observations to numerical simulations of stellar halo formation requires a straightforward definition for the ‘abundance of substructure’, one that can be quantified with a method equally applicable to simulations and observations. Algorithms already exist for identifying substructure in huge multidimensional data sets (e.g. Sharma & Johnston 2009), such as the data expected from *Gaia* supplemented by chemical abundance measurements (Freeman & Bland-Hawthorn 2002). These algorithms can also be applied to simulations, although this

is not straightforward. One problem is that current (cosmological) hydrodynamic simulations still fall short of the star-by-star ‘resolution’ of the *Gaia* data, particularly in the solar neighbourhood (e.g. Brown, Velázquez & Aguilar 2005).

In the outer halo, longer mixing times allow ancient structures to remain coherent in configuration space for many Gigayears. However, six-dimensional *Gaia* data will be restricted to relatively bright stars. In the near future, studies of the outer halo (beyond  $\sim 20$  kpc) will continue to rely on a more modest number of ‘tracers’ (giant and horizontal branch stars). For these stars, typically only angular positions and (more uncertain) estimates of distance and radial velocity are available. In this regime, current simulations contain as many particles as there are (rare) tracer stars in observational samples, and can be compared directly with data that are already available. Here we focus on quantifying the degree of structure in rare tracer stars with a generic method, which we apply to observational data and to simulations of MW-like stellar haloes.

Most studies of spatial and kinematic structure in the MW halo have given priority to the discovery of individual overdensities (exceptions include Gould 2003; Bell et al. 2008; Xue, Rix & Zhao 2009; Helmi et al. 2011; Xue et al. 2011). Relatively few have investigated global statistical quantities for the entire stellar halo, although several authors have suggested an approach based on clustering statistics. Re Fiorentin et al. (2005) analysed the velocity–space clustering of a small number of halo stars in the solar neighbourhood, using a correlation function statistic. Following early work by Doinidis & Beers (1989), Brown et al. (2004) examined the

\*E-mail: acooper@mpa-garching.mpg.de

angular two-point correlation function of photometrically selected blue horizontal branch (BHB) stars in the Two Micron All Sky Survey, probing from  $\sim 2$  to 9 kpc. They detected no significant correlations at latitudes  $|b| \gtrsim 50^\circ$ , but did detect correlations on small scales ( $1^\circ$ ,  $\sim 100$  pc) at lower latitudes, which they attributed to structure in the thick disc. Lemon et al. (2004) performed a similar analysis for nearby F-type stars in the Millennium Galaxy Catalogue and found no significant clustering.

Starkenburg et al. (2009) used a correlation function in *four* dimensions to identify substructures in the Spaghetti pencil-beam survey of the distant halo (Dohm-Palmer et al. 2000; Morrison et al. 2000). With this method they obtained a significant detection of clustering and set a lower limit on the number of halo stars in all substructures. Similarly, Schlaufman et al. (2009) constrained the mass fraction of the halo in detectable substructure by estimating the completeness of their overdensity detection algorithm. Starkenburg et al. and Schlaufman et al. concluded that  $>10$  (by number of stars) and  $\sim 30$  per cent (by volume) of the MW halo belongs to groups meeting their respective definitions of phase-space substructure. These methods were tested on ‘mock catalogues’ of tracer stars based on simplified models of the stellar halo.

The work of Xue et al. (2009, 2011) is particularly relevant. Xue et al. (2009) considered the pairwise radial velocity separation of a sample of 2558 halo BHB stars as a function of their separation in space, but found no evidence of clustering. From comparisons to the simulations of Bullock & Johnston (2005), Xue et al. concluded that a pairwise velocity statistic was not capable of detecting structure against a more smoothly distributed background in phase space (made up from stars in phase-mixed streams). However, their observed signal was not compared to an expected signal from random realizations. More recently, Xue et al. (2011) studied an enlarged catalogue of BHBs comprising more than 4000 stars. They quantified clustering in this larger sample using a four-dimensional metric (similar to that of Starkenburg et al. 2009), finding a significant excess of clustering on small scales by comparison to smooth models. The conclusions of this more recent study by Xue et al. agree with our own, as we discuss further in Section 7.

The statistic we develop in this paper also builds on the approach of Starkenburg et al. (2009). We define a two-point correlation function based on a metric combining pairwise separations in four readily obtained phase-space observables for halo stars (angular position, radial distance and radial velocity). We apply this statistic to the catalogue of BHB stars published by Xue et al. (2008)<sup>1</sup> and demonstrate that a significant clustering signal can be recovered from these data.

A clustering metric of the kind we propose can be tuned to probe a specific scale in phase space by adjusting the weight given to each of its components. In the stellar halo, however, many ‘components’ may be superimposed with a complex assortment of scales and morphologies in phase space (Johnston et al. 2008; Cooper et al. 2010). For this reason, it is not clear, *a priori*, what sort of signal to expect, or which scales are most relevant. We find that we cannot identify an ‘optimal’ metric. Instead, we make a fiducial choice based on the self-consistent accreted halo models of Cooper et al. (2010). These incorporate an *ab initio*  $\Lambda$ CDM galaxy formation model using high-resolution cosmological *N*-body simulations from the Aquarius project (Springel et al. 2008). We apply our fiducial metric to the data and to these models. We find that even though

both the metric and our choice of scaling are simple, this approach has the power to discriminate quantitatively between qualitatively different stellar haloes.

We describe the basis of our method in Section 2 and the Sloan Digital Sky Survey (SDSS) Data Release 6 (DR6) BHB catalogue of Xue et al. (2008) in Section 3. In Section 4 we describe our simulations (Section 4.1) and our procedure for constructing mock catalogues (Section 4.2). Section 5 describes our choice of a fiducial metric. In Section 6 we apply our method to quantify clustering in the SDSS data and compare this with our mock catalogues. Our conclusions are given in Section 7.

## 2 A METRIC FOR PHASE-SPACE DISTANCE

The most readily obtained phase-space observables for halo stars are their Galactic angular coordinates,  $l$  and  $b$ , heliocentric radial distance,  $r_{\text{hel}}$ , and heliocentric line-of-sight velocity,  $v_{\text{hel}}$ . Using its angular position and distance estimate, each star can be assigned a three-dimensional position vector in Galactocentric Cartesian coordinates,  $\mathbf{r}$  ( $X, Y, Z$ ), and a radial velocity corrected for the solar and local standard of rest motions,  $v$ . We begin by defining a scaling relation (metric),  $\Delta$ , which combines these observables into a simple ‘phase-space separation’ between two stars:

$$\Delta_{ij}^2 = |\mathbf{r}_i - \mathbf{r}_j|^2 + w_v^2(v_i - v_j)^2. \quad (1)$$

Here,  $|\mathbf{r}_i - \mathbf{r}_j|$  is the separation of a pair of stars in coordinate space (in kiloparsec), and  $v_i - v_j$  is the difference in their radial velocities (in kilometre per second). The scaling factor  $w_v$  has units of  $\text{kpc km}^{-1} \text{s}$ , such that  $\Delta$  has units of kpc. The choice of  $w_v$  is arbitrary unless a particular ‘phase-space scale’ of interest can be identified. This is not straightforward; we discuss some possible choices below.

The aim of this paper is to explore  $\xi(\Delta)$ , the cumulative two-point correlation function of halo stars in the metric defined by equation (1). Throughout, we use the estimator

$$1 + \xi(\Delta) = \frac{DD(<\Delta)}{\langle RR(<\Delta) \rangle}. \quad (2)$$

Here  $DD(<\Delta)$  counts the number of pairs in the sample separated by less than  $\Delta$ , and  $\langle RR(<\Delta) \rangle$  is the equivalent count for pairs of random points within the survey volume, averaged over several realizations. To generate these realizations we ‘shuffle’ the data by randomly reassigning  $(r_{\text{hel}}, v_{\text{hel}})$  pairs to different  $(l, b)$  coordinates drawn from the original catalogue.<sup>2</sup>

Similar methods for quantifying the clustering of stars in a four-dimensional space are described by Starkenburg et al. (2009, applied to a sample of giant stars from the Spaghetti survey) and Xue et al. (2011, applied to a sample of BHB stars from SDSS). Our  $\Delta$  metric is very similar to the  $\delta_{4d}$  metric of Starkenburg et al. in the limit of small angular separations.<sup>3</sup> We have verified that our metric gives

<sup>2</sup> The same randomization procedure was used by Starkenburg et al. (2009). Xue et al. (2011) use a similar procedure, but for each galaxy they reassign  $r_{\text{hel}}$  and  $v_{\text{hel}}$  separately to different  $(l, b)$  coordinates.

<sup>3</sup> Starkenburg et al. developed their metric with the aim of identifying ‘true’ pairs of stars with high confidence. In their definition (equation 1 of Starkenburg et al. 2009), the  $\delta_{4d}$  separation between two stars depends not only on their actual phase-space coordinates, but also on how accurately those coordinates are measured. For example, moving two stars 10 kpc further apart and simultaneously decreasing the error on their distance measurements by a factor of 10 (relative to the average of the sample) results in the same  $\delta_{4d}$ . Thus  $DD/RR$  for separations in  $\delta_{4d}$  is not a straightforward measurement of physical clustering.

<sup>1</sup> The larger sample used by Xue et al. (2011) was not publicly available at the time this paper went to press.

similar results when we repeat the analysis of Starkenburg et al. using the Spaghetti sample of 101 halo red giant branch stars. For the rest of this paper we will focus on clustering in the SDSS DR6 BHB catalogue of Xue et al. (2008).

### 3 OBSERVATIONAL DATA

Xue et al. (2008) have published a catalogue of 2558 stars from SDSS DR6, which they identify as high-confidence halo BHBs (contamination <10 per cent) using a combination of colour cuts and Balmer line diagnostics. This sample ranges in distance from 4 to 60 kpc; a cut on distance error excluded more distant stars observed in SDSS. Xue et al. (2008) claim distance errors of  $\sim 10$  per cent and radial velocity errors of 5–20 km s $^{-1}$ . This catalogue is not a complete sample of halo BHBs. In particular, Xue et al. note that the targeting of SDSS spectroscopy is biased against the follow-up of more distant stars.

To isolate stars representing the kinematics of the halo (in order to study the Galactic circular velocity profile) Xue et al. (2008) further restricted their sample to stars at heights  $|z| > 4$  kpc above the plane (avoiding the thick disc). We also apply this cut (which excludes thick disc stars and low-latitude halo stars alike), leaving 2401 stars in the sample. Finally, we exclude nine stars in the sample identified by Xue et al. (2009) as probable globular cluster members. Thus, the sample against which we compare our models contains 2392 stars from the 2558 stars in the Xue et al. (2008) catalogue. The effects of these refinements to the sample on the recovered  $\xi(<\Delta)$  signal are discussed in Section 6.1.

## 4 STELLAR HALO SIMULATIONS

### 4.1 N-body and galaxy formation model

The mock observations that we use to test the  $\xi(<\Delta)$  correlation function are derived from simulations of the accreted stellar halo presented in Cooper et al. (2010). These simulations approximate the dynamics of stars in dwarf satellites of MW-like galaxies by ‘tagging’ appropriate particles (i.e. those strongly bound within subhaloes) in the Aquarius suite of high-resolution  $N$ -body simulations (Springel et al. 2008). Each ‘tag’ associates a dark matter (DM) particle with a particular stellar population of a given mass, age and metallicity. This ‘tagging’ technique is reasonable in the regime of high mass-to-light ratios, which is supported in this case by observations of stellar kinematics in dwarf galaxies (e.g. Walker et al. 2009).

The tagging method has a single free parameter, the fraction of the most-bound particles chosen in each DM halo for each assignment of newly formed stars (for further details see Cooper et al. 2010). The value of this parameter (1 per cent) was fixed by requiring the population of surviving satellites (at the present day) to have a distribution of half-light radius as a function of luminosity consistent with MW and M31 observations.<sup>4</sup> The Cooper et al. models differ from the earlier models of Bullock & Johnston (2005) in that they treat the full cosmological evolution of all satellites self-consistently in a single  $N$ -body simulation, and use a comprehensive semi-analytic model of galaxy formation (Bower et al. 2006) constrained by data on large scales and compatible with the observed

<sup>4</sup> The luminosity function of surviving satellites in these models also agrees with MW and M31 data. This agreement is mostly due to the underlying galaxy formation model.

MW satellite luminosity function. Both the Cooper et al. and the Bullock & Johnston simulations produce highly structured stellar haloes built from the debris of disrupted dwarf galaxies. As we discuss further below, other halo components formed *in situ* may be present in real galaxies (e.g. Abadi, Navarro & Steinmetz 2006; Zolotov et al. 2009; Font et al. 2011) but these are expected to be more smoothly distributed than the accreted component (e.g. Helmi et al. 2011).

As in Springel et al. (2008) and Cooper et al. (2010), we refer to our six simulations as haloes Aq-A, Aq-B, Aq-C, Aq-D, Aq-E and Aq-F. From these simulations, we construct catalogues of tracer stars (BHB stars, for example) by converting the stellar mass assigned to each dark matter particle into an appropriate number of stars.

Each DM particle can give rise to many tracer stars if it is tagged with sufficient stellar mass. We therefore interpolate the positions and velocities of these tracer stars between nearby tagged DM particles. To accomplish this, the 32 nearest phase-space neighbours of each tagged particle are identified using a procedure which we describe below. The mean dispersion in each of the six phase-space coordinates is then calculated for each particle as an average over its neighbours. These dispersions define a six-dimensional ellipsoidal Gaussian kernel centred on the particle, from which the positions and velocities of its tracer stars are drawn randomly. Each progenitor galaxy (a set of tagged DM particles accreted by the main ‘MW’ halo as members of a single subhalo) is treated individually in this smoothing operation, i.e. particles are smoothed using only neighbours from the same progenitor (so there is no ‘cross-talk’ between streams from different progenitors). This procedure can be thought of as a crude approximation to running our original simulation again including each tracer star as a test particle.

The ‘distance in phase space’ used to identify neighbours in the interpolation scheme is defined by a scaling relation between distances in configuration space and velocity space.<sup>5</sup> For each progenitor, we adopt an individual scaling which corresponds to making the median pairwise interparticle separation of its particles in configuration space (at  $z = 0$ ) equal to their median separation in velocity space. In practice, the value of this scaling parameter makes very little difference to the results we present, when compared to the extreme choice of selecting only 32 velocity or position neighbours (disregarding the other three coordinates in each case). Giving more weight to configuration-space neighbours smears out velocity substructure within the debris of a progenitor (e.g. where two wraps of a stream pass near one another). Giving more weight to velocity neighbours has the opposite effect – stars can be interpolated over arbitrarily large separations in configuration space, but coherent velocity structures are preserved. Therefore, the ‘optimal’ choice is the scaling which balances smoothing in configuration space against smoothing in velocity space.

To quantify this balance between smoothing in configuration and velocity space, we compute six smoothing lengths for each particle,  $\epsilon_{x,i}$  and  $\epsilon_{v,i}$ , where  $i$  represents a single dimension in space or velocity. To compute these dispersions, we use the 32 nearest phase-space neighbours of each particle. We define the ‘optimum’ choice of scaling for each progenitor galaxy as that which minimizes the

<sup>5</sup> In this part of the calculation, we are only interested in finding neighbours, so the absolute values of these distances are not important. This scaling of velocity space to configuration space for the purpose of resampling the simulations should not be confused with the  $\Delta$  metric we define for our analysis of clustering.

quantity

$$\sigma_\epsilon^2 = \left( \frac{1}{\bar{\epsilon}_{x,\min}} \sum_{i=0}^3 \epsilon_{x,i} \right)^2 + \left( \frac{1}{\bar{\epsilon}_{v,\min}} \sum_{i=0}^3 \epsilon_{v,i} \right)^2. \quad (3)$$

This is the sum in quadrature of the mean smoothing lengths in configuration and velocity space, normalized, respectively, by  $\bar{\epsilon}_{x,\min}$ , the ‘minimal’ mean smoothing length in configuration space (obtained from the 32 nearest configuration space neighbours) and  $\bar{\epsilon}_{v,\min}$ , the ‘minimal’ mean smoothing length in velocity space (obtained from the 32 nearest velocity-space neighbours). We find that the scaling obtained by matching the median interparticle separations in position and velocity as described above is typically a good approximation to this optimal value – a similar result is discussed in more detail by Maciejewski et al. (2009).

In the Cooper et al. model, when a given stellar population is formed, the most bound 1 per cent of DM particles in the corresponding dark halo at that time are chosen as dynamical tracers of that population. Hence, each DM particle to which stars are assigned has an individual mass-to-light ratio,  $M/L$ , which can be as high as  $\sim 1$  (i.e.  $M_{\text{stellar}} \sim 10^4 M_\odot$ ) and as low as  $\sim 10^{-6}$ . This will affect the density of stars seeded by a DM particle independently of the density of its neighbours in phase space (i.e. a low  $M/L$  particle will create a denser ‘cluster’ of tracers relative to a high  $M/L$  particle with the same neighbouring positions and velocities). We have tested an alternative approach in which the  $M/L$  of each particle in a given progenitor is resampled by distributing the total stellar mass of the progenitor evenly amongst its tagged particles.<sup>6</sup> We find that the extra clustering due to a few ‘hot’ particles in our default approach makes no difference to our results.

## 4.2 Tracer stars and mock observations

Each  $N$ -body dark matter particle in our simulation contributes a number of tracer stars to our mock observations, based on the stellar population with which it has been ‘tagged’. In the specific case of our comparisons to SDSS, these tracers are BHB stars meeting the selection criteria of Xue et al. (2008). Here we assume a global scaling between the stellar mass associated with each  $N$ -body particle,  $M_*$ , and the number of BHBs it contributes to our mock catalogues, i.e.  $N_{\text{BHB}} = f_{\text{BHB}} M_*$ , where  $f_{\text{BHB}}$  is the number of tracer stars per unit mass of the original stellar population.<sup>7</sup> For each  $N$ -body particle, the actual number of BHB stars generated is drawn from a Poisson distribution with mean  $N_{\text{BHB}}$ . The correlation function results described below are not sensitive to the choice of  $f_{\text{BHB}}$ , provided that the underlying distribution is well sampled at a given scale. We have therefore selected a fiducial value of  $f_{\text{BHB}}^{-1} = 3000 M_\odot \text{ star}^{-1}$ . In creating the mock catalogue, we do not include

<sup>6</sup> This is almost equivalent to choosing  $M/L$  only once, at the time in the simulation when the progenitor falls into the main halo (similar to the lower resolution model of De Lucia & Helmi 2008).

<sup>7</sup> We do this because we prefer to make a straightforward comparison with the observational data in this paper. In principle, the age and metallicity information associated with each stellar population in our model could be used to populate an individual colour-magnitude diagram for each  $N$ -body particle, and make a detailed prediction for the appropriate number of tracers. The ‘bias’ of BHBs relative to the total stellar mass distribution of the halo (Bell et al. 2010) may affect the clustering statistic recovered (Xue et al. 2011), but this effect is beyond the scope of the present paper.

any stars gravitationally bound to satellites. However, we do include stars in their tidal tails (which, by our definition, are part of the stellar halo).

Using our simulated BHB catalogues, we create mock observations for comparison to the Xue et al. (2008) data as follows. First, we located the observer at a radius  $r_\odot = 8 \text{ kpc}$  from the centre of the halo. For our main comparison to the data, we restrict all observers to the same ‘Galactic plane’, with each random vantage point differing only in its azimuthal angle in this plane and in the ‘polarity’ of the Galactic rotation axis (the  $Z$  coordinate). However, the orientation of the rotation axis cannot be directly constrained by the simulation, which only models the *accreted* component of the halo and the bulge, and not the *in situ* formation of a stellar disc. As described in Cooper et al. (2010), the accreted ‘bulge’ is prolate or mildly triaxial. We define the minor axis of this bulge component (conservatively defined by all accreted stars within  $r < 3 \text{ kpc}$ ; Cooper et al. 2010) as the Galactic  $Z$ -axis. This axis is essentially identical to the minor axis of the dark halo within  $r < 3 \text{ kpc}$ . There are other plausible choices of Galactic plane (e.g. relative to the shape or spin vectors of the entire dark halo, rather than the stars in its inner regions). However, any choice is somewhat arbitrary without a self-consistent simulation of disc formation.<sup>8</sup>

Having chosen a location for the observer, we select all tracer stars within the spectroscopic footprint of SDSS DR6 having Galactocentric distance in the range 20–60 kpc (our principal comparison will focus on the outer halo as defined by this distance range, although we also study the ranges 5–60 and 5–20 kpc below). Galactic longitude and latitude are defined such that  $(l, b) = (0, 0)$  is the vector directed from the observer to the centre of the halo. We set the heliocentric velocity components of each star assuming a solar motion of  $U, V, W = (10.0, 5.2, 7.2) \text{ km s}^{-1}$  (Dehnen & Binney 1998) and a velocity of the local standard of rest about the Galactic Centre  $v_{\text{LSR}} = 220 \text{ km s}^{-1}$ . We compute  $(X, Y, Z)$  and  $v_{\text{los}}$  as described by Xue et al. (2008). Finally, distances and velocities are convolved with Gaussian observational errors of  $\sigma_d = 10 \text{ per cent}$  and  $\sigma_v = 15 \text{ km s}^{-1}$ , respectively (Xue et al. 2008).

In both the mock observations and the real data, the average random pair count  $\langle RR \rangle$  is calculated by reshuffling distances and velocities among the positions on the sky of stars many times. We find that by using 500 random catalogues to calculate  $\langle RR \rangle$  for each mock observation and performing 500 mock observations in each halo, we obtain a sufficiently well-converged estimate of the distribution of  $\xi(<\Delta)$ .

Fig. 1 illustrates the structure of one of our haloes and verifies that our mock observations can result in distributions of heliocentric distance and heliocentric radial velocity similar to the SDSS data of Xue et al. (2008). In this figure we have specifically chosen an observer orientation in halo Aq-A such that the distributions of distance and velocity we recover are close to those of the data, after convolution with typical observational errors. We have aligned the Galactic  $Z$ -axis of the mock observer with the minor axis of the dark halo, as described above. This confines the most prominent structures in the stellar halo to low Galactic latitudes, outside the SDSS DR6 spectroscopic footprint. Of course, the simulated haloes

<sup>8</sup> In a full hydrodynamic simulation the effects of feedback and adiabatic contraction may also make the dark halo itself more spherical (e.g. Abadi et al. 2010; Tissera et al. 2010).

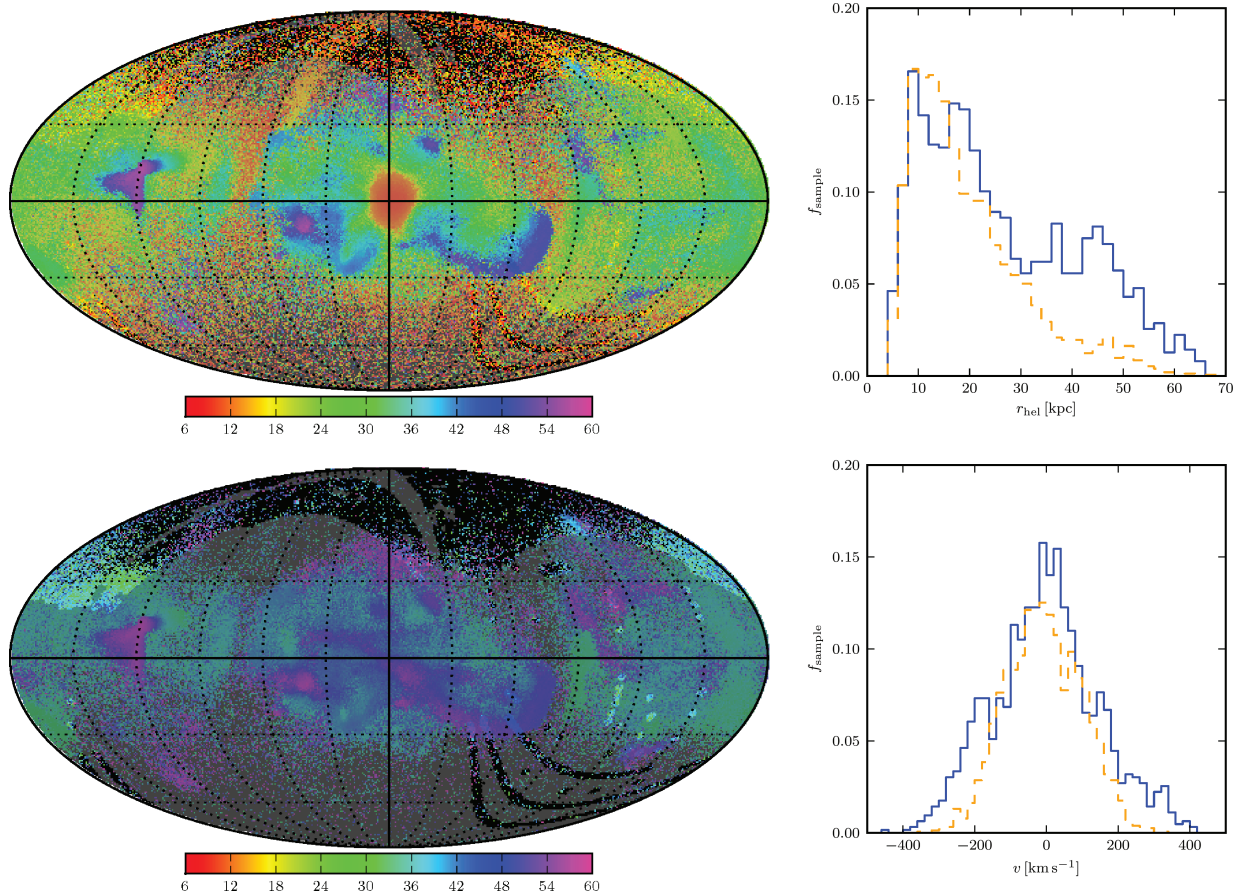


**Figure 1.** Left-hand panels: an example of the sky distribution of halo BHB stars in Aq-A from the perspective of a ‘solar’ observer, shown as Mollweide projections in Galactic coordinates centred on  $(l, b) = (0, 0)$ . Colours indicate the mean heliocentric distance of stars in each pixel, in kiloparsec. Pixels outside the SDSS DR6 footprint are shown with lower contrast. The upper panel includes all BHB stars from 6–60 kpc, the lower panel includes only stars in the range 30–60 kpc. Our fiducial choice of the Galactic Z-axis with respect to the dark halo has been applied, but distances in these panels are not convolved with observational errors. The normalization of BHB stars per unit stellar mass in the halo has been increased in these panels to emphasize the distribution of structure. Right-hand panels: blue histograms show the distribution of heliocentric distances (above) and heliocentric velocities (below) for the fiducial observer corresponding to the left-hand panels, after convolution with observational errors (see text). Orange histograms are the distributions for stars in the Xue et al. (2008) catalogue. To compare the shape of the two distributions, the normalization of the mock distributions in these panels has been matched to that of the observations for  $r < 20$  kpc, where the observations are most likely to be complete.

are inhomogeneous on large scales, and there are many choices of observer in each halo that *do not* resemble the SDSS data.<sup>9</sup>

## 5 DISTANCE-VELOCITY SCALING IN THE $\Delta$ METRIC

Before  $\xi(<\Delta)$  can be computed, a value must be chosen for the velocity-to-distance scaling  $w_v$  in equation (1). There is no clearly well-motivated way to choose this value, and in the absence of a physical justification, it must be treated as a free parameter. The choice of  $w_v$  determines the scale of substructure to which the correlation function is most sensitive. Naively, we expect this to be the typical width and transverse velocity dispersion of a ‘stream’.

<sup>9</sup> As discussed by Xue et al. (2008), the completeness of the data declines at larger distances ( $r_\odot > 20$  kpc). Mock catalogue distributions that match the observed distributions well at  $r_\odot < 20$  kpc typically show a flatter profile with identifiable overdensities (streams) at larger distances. As the SDSS spectroscopic selection function for the data we use is difficult to quantify (Xue et al. 2008), we do not explore the effects of incompleteness in this paper.

It is preferable to fix this parameter in a universal manner that does not depend on the details of a particular survey. We make a fiducial choice of  $w_v$  as follows.

In each simulated halo we adopt the SDSS-like survey configuration described in Section 4.2 (without observational errors or assumptions about the orientation of the Galactic plane). We construct one-dimensional distributions of the separation in radial distance and velocity between stars. We generate many random realizations of these distributions by first convolving each simulated star with Gaussian smoothing kernels of width 8 kpc (distance) and 80 km s<sup>-1</sup> (velocity), and then drawing randomly from these ‘smoothed’ distributions. The smoothing scales were chosen as a compromise between signal (diminished by oversmoothing) and noise (increased by undersmoothing). Using these random realizations we construct one-dimensional correlation functions for each distribution. These two correlation functions are shown for halo Aq-A in Fig. 2. Although the signals are intrinsically weak, they have a very similar shape for both distributions, each with a characteristic ‘turnover’ scale. Matching this scale in the two correlation functions corresponds to  $w_v \sim 0.04 \pm 0.01$  kpc km<sup>-1</sup> s for the six haloes, which we adopt as a fiducial value. We caution that although the scales

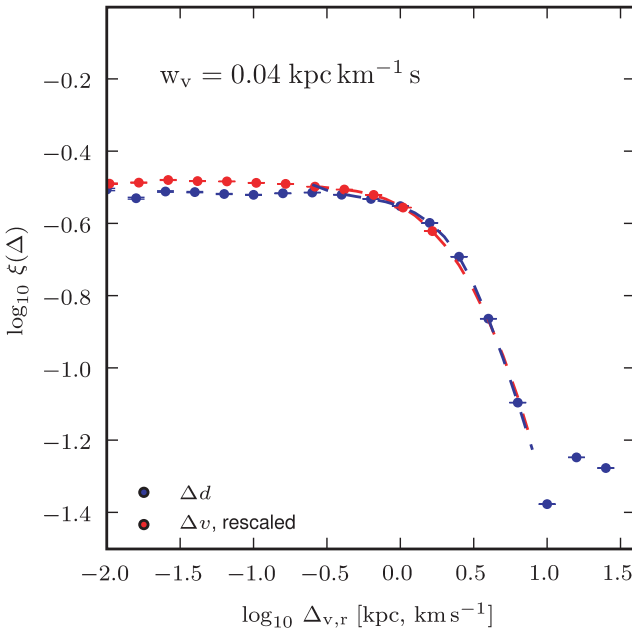


**Figure 2.** Correlation functions in spatial separation (blue) and velocity separation (red) for stars in halo Aq-A. The velocity separation correlation function has been scaled by a factor  $w_v = 0.04 \text{ kpc km}^{-1} \text{s}$  to match the turnover in the configuration space separation correlation function.

on which we match the one-dimensional correlation functions are somewhat smaller than the smoothing scales we adopt to create the random distributions, this does not guarantee that our choice of  $w_v$  is unaffected by our choice of smoothing.

Clearly, there are other ways of fixing  $w_v$ . In practice, however, our conclusions are not highly sensitive to the value of this parameter. Values of the order of  $w_v \sim 0.01\text{--}1.0 \text{ kpc km}^{-1} \text{s}$  result in very similar  $\xi(\Delta)$  correlation functions. Values lower than  $0.01 \text{ kpc km}^{-1} \text{s}$  recover very little signal. Values above  $1 \text{ kpc km}^{-1} \text{s}$  treat  $1 \text{ km s}^{-1}$  velocity differences as equivalent to  $>1 \text{ kpc}$  separations in space, and so make the cumulative correlation function very noisy on small scales for only a marginal increase in the overall signal. (This noise, in turn, increases the scatter between signals measured by different observers.) We find that our choice of  $w_v \sim 0.04 \text{ kpc km}^{-1} \text{s}$  is a reasonable compromise. Our method for choosing  $w_v$  can be compared with that of Starkenburg et al. (2009), who determine the equivalent of  $w_v$  in their metric to be the ratio of the Spaghetti survey limits in radial distance and velocity ( $0.26 \text{ kpc km}^{-1} \text{s}$ ). Either value is acceptable to illustrate our approach and compare to simulations. We therefore adopt  $w_v \sim 0.04 \text{ kpc km}^{-1} \text{s}$ .

## 6 CLUSTERING OF SDSS BHB STARS

### 6.1 Clustering in the Xue et al. sample

Fig. 3 shows  $\xi(<\Delta)$  computed for 2392 BHB stars in the Xue et al. (2008) sample (Section 3; grey points). Stars at small separations in the metric of equation (1) ( $\Delta < 4 \text{ kpc}$ ) show significant clustering. The amplitude of the signal increases if we restrict the sample to larger Galactocentric distances,  $r > 20 \text{ kpc}$  (black points). At larger distances substructure is expected to be dynamically young and to have undergone less phase mixing. Our finding of stronger clustering for more distant halo stars is in qualitative agreement with the results of Xue et al. (2011).

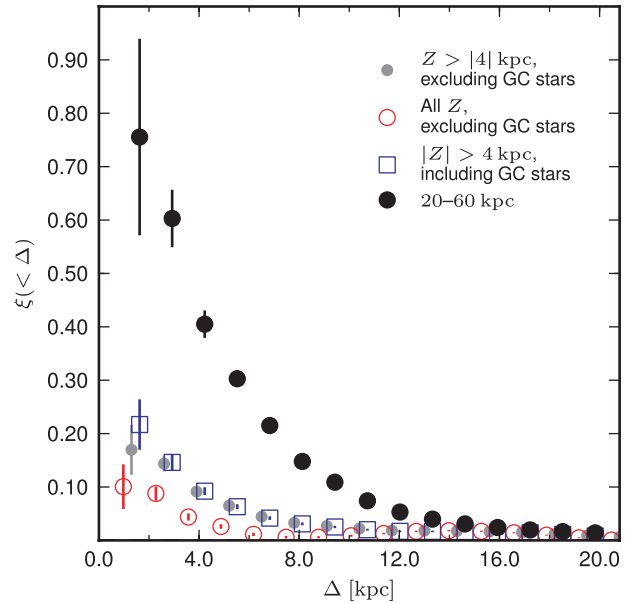


**Figure 3.**  $\xi(<\Delta)$  correlation function for the SDSS BHB sample of Xue et al. (2008). Black points (with Poisson error bars) show  $\xi(<\Delta)$  computed for all stars at Galactocentric distances greater than  $20 \text{ kpc}$ . Grey points show the result for all stars in the main sample (Galactocentric distances of  $4\text{--}60 \text{ kpc}$ ). The blue squares include nine stars suspected to belong to globular clusters, while red circles include stars at low Galactic  $|z|$  heights (possible thick disc stars). Neither of these contributions is relevant for the more distant selection shown by the black points.

Although we appear to recover a significant clustering signal in Fig. 3, we have only one SDSS. The observed signal may be an artefact of the particular structures covered by the SDSS footprint. Other parts of the halo may be smoother or more structured, or may appear so when viewed from different points around the solar circle. We will address this issue of sample variance in the following section using our mock catalogues.

We show two further permutations of the Xue et al. (2008) sample in Fig. 3. The first of these (red open circles) includes stars close to the Galactic plane,  $|Z| < 4 \text{ kpc}$ . These were excluded from the main sample of Xue et al. (2008) to excise the thick disc.

Although only  $\sim 150$  stars are excluded by the cut on  $|Z|$ , they make a substantial difference to the correlation function, suppressing the clustering signal on scales below  $\Delta < \sim 8 \text{ kpc}$ . In the SDSS data the majority of low- $|Z|$  stars are at small heliocentric radii. These stars constitute a foreground ‘screen’ with a relatively smooth distribution, which may dilute the signal of correlated stars.

The final sample shown in Fig. 3 (blue open squares) includes all stars from the main sample (grey points) and a further nine BHB stars identified as globular cluster members by Xue et al. (2009). Two of these are from one cluster, and seven from another. Including these stars marginally increases the clustering signal in the smallest separation bin. This shows that the technique is sensitive to the clustering of stars on these scales, which correspond to separations comparable to the distance and velocity errors of the data.

### 6.2 Comparison with mock catalogues

In Fig. 4 we show the range of  $\xi(<\Delta)$  measured for each of the six simulations described in Section 4, overplotting the data shown in Fig. 3. As described in Section 4.2 these results correspond to mock BHB catalogues for 500 solar observers located in the ‘Galactic

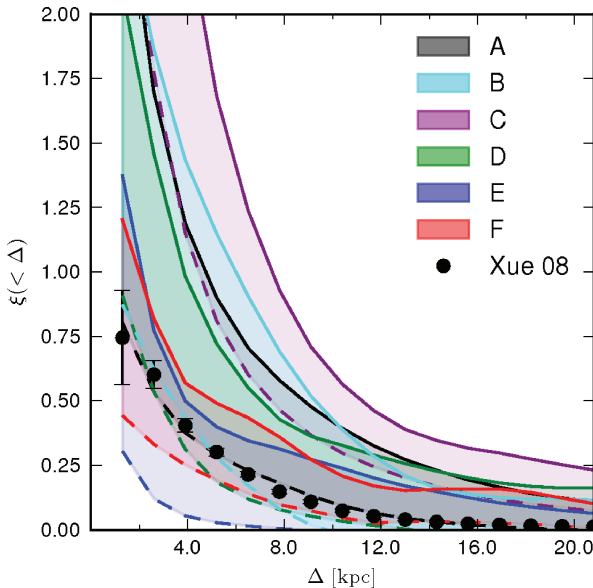


**Figure 4.**  $\xi(<\Delta)$  for halo stars of Galactocentric distances  $20 < r < 60$  kpc, computed for 500 observers in the six Aquarius simulations of Cooper et al. (2010). Coloured regions (delineated by dashed and solid lines) indicate the 10–90 per cent range of  $\xi(<\Delta)$  in each bin of  $\Delta$ , for each halo. All observers are restricted to the Galactic plane, and distances and velocities are convolved with observational errors (see text). Black points with error bars reproduce the observed BHB  $\xi(<\Delta)$  shown in Fig. 3.

plane', with typical observation errors in distance and velocity. The dashed and solid lines bounding each coloured region in Fig. 4 correspond to the 10th and 90th percentile values we obtain in each bin of  $\xi(<\Delta)$ . At a given scale in our  $\Delta$  metric, the strength of the clustering signal varies considerably from halo to halo and between individual observers.

The overall trend of  $\xi(<\Delta)$  is similar to the observations in all haloes, although the clustering signal rises more steeply on small scales in most of the simulations. On scales  $\Delta < 4$  kpc, significant clustering is detected by all observers in five of the six haloes. The exception is halo Aq-E (dark blue). This stellar halo is highly

concentrated, and at  $r > 20$  kpc is dominated by a single radial stream (see figs 6 and 7 of Cooper et al. 2010).

We find that two haloes, Aq-E and Aq-F (red), are consistent with the observed  $\xi(<\Delta)$  on all scales. The structure of Aq-F is atypical for the sample – most of its stars are accreted in a late 3:1 merger and its surface brightness at the solar radius is substantially higher than current estimates for the MW halo. In projection, Aq-F resembles the 'shell'-dominated haloes observed in a number of nearby elliptical galaxies. Meanwhile haloes Aq-A (black), Aq-B (cyan) and Aq-D (green) are marginally inconsistent with the data: below  $\Delta \sim 4$  kpc, ~90 per cent of mock observations in these haloes imply a greater degree of clustering than we find for the MW, particularly on small scales. Aq-C (purple) is entirely inconsistent with the MW observations on all scales, showing a much higher degree of clustering. Beyond 20 kpc, the sky of an observer in Aq-C is dominated by two bright tidal streams on wide ( $\sim 100$  kpc) orbits. Although their orbital planes are approximately coincident with our definition of the Galactic plane, nevertheless sections of these streams intrude on the SDSS footprint at low Galactic latitudes.

The DR6 footprint and the cut on extraplanar height in the Xue et al. (2008) sample exclude stars near the Galactic plane from our clustering analysis. Fig. 5 illustrates how our definition of the Galactic plane influences the halo clustering signal. In panel (a) the orientation of the Galactic plane with respect to the halo is chosen randomly for each of the 500 mock observers (i.e. observers are distributed over a sphere of radius  $r_\odot = 8$  kpc), whereas in panel (b) the Galactic Z direction is aligned with the minor axis of the halo for all observers as in Fig. 4. To focus on the effects of this alignment, the distances and velocities of stars in these two panels have *not* been convolved with observational errors.

The systematically higher clustering signals in panel (b) of Fig. 5 suggest that the plane perpendicular to the minor axis of the dark matter halo is special. In Cooper et al. (2010) and above, we have noted the strong correlation between the shape of the dark halo and the inner regions of the stellar halo. This alignment of halo structure also extends, more loosely, to other prominent stellar halo structures at large distances. An overall flattening of the stellar halo arises because our dark matter haloes are embedded in long-lived filaments of the cosmic web. Typically one or two such filaments dominate the infall directions of both satellite galaxies and smoothly

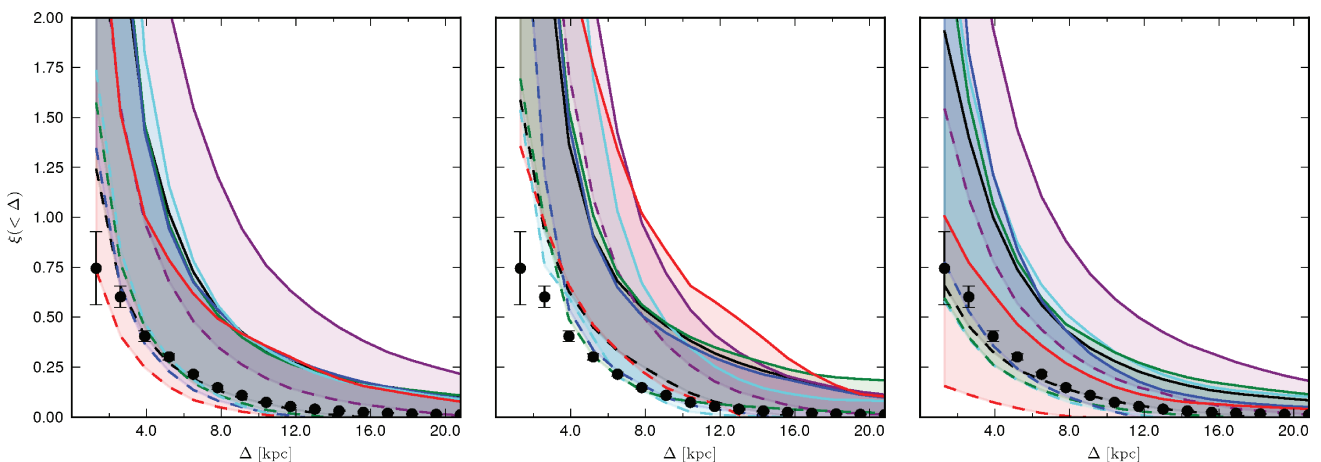


**Figure 5.**  $\xi(<\Delta)$  for mock observations, as Fig. 4. From left to right, we vary our modelling assumptions as follows: (a) no restriction on the alignment of the Galactic plane with respect to the dark halo (the observer is located randomly on a sphere of radius  $r_\odot = 8$  kpc) and no convolution of the data with the expected observational errors; (b) the observer is restricted to the Galactic plane as in Fig. 4, but the mock observations are *not* convolved with expected observational errors; (c) as panel (a), but mock observations *are* convolved with errors. Colours are as Fig. 4.

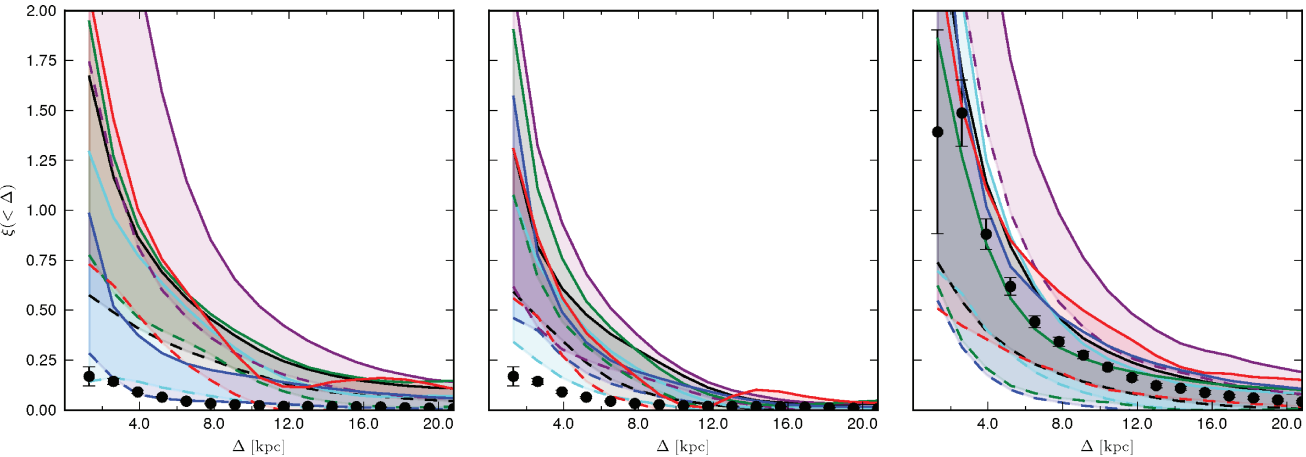


**Figure 6.**  $\xi(<\Delta)$  for mock observations, as Fig. 4. Here we select three different Galactocentric distance ranges in the halo: from  $5 < r < 60$  kpc (left-hand panel), from  $5 < r < 20$  kpc (central panel) and from  $30 < r < 60$  kpc (right-hand panel). The MW BHB clustering signal (black points) is recalculated for the distance range in each panel. Colours are as Fig. 4.

accreted dark matter, which also contributes to the shape of the dark halo (e.g. Libeskind et al. 2005; Lovell et al. 2011; Vera-Ciro et al. 2011; Wang et al. 2011). The distribution of stars stripped from infalling satellites echoes the large-scale correlation of their orbital planes.

Because of this flattened global structure, the distribution of halo stars in our choice of Galactic plane tend to be more smoothly distributed (i.e. this plane contains more diffuse phase-mixed material as well as coherent substructure). Panel (b) demonstrates how the ‘contrast’ of small-scale substructure in the outer halo is enhanced when these smoother components are excluded from the clustering analysis (through a combination of the SDSS footprint and the cut on  $|Z|$ ). This is particularly true in the case of Aq-F, where the majority of the mass in the halo is contributed by one extensive and relatively ‘smooth’ component. By contrast, in Aq-C the average clustering amplitude *decreases* on large scales when we fix the Galactic plane. As noted above, in this case the massive coherent streams that dominate the clustering signal of this halo mostly fall outside the SDSS footprint.

Panel (c) of Fig. 5 shows the randomly aligned observations of panel (a) convolved with observational errors in distance and velocity. These errors ‘smooth out’ the halo, suppress the clustering signal overall and increase the variance between observers on small scales. Again the effect is most pronounced for Aq-F, where blurring of the dominant smooth component further decreases the contrast of substructure. In most cases these two effects (alignment and observational errors) counteract each other to produce the distribution of signals shown in Fig. 4. In the case of Aq-E the signal suffers disproportionately from errors in the aligned configuration, perhaps because this signal is due to a small number of pairs at large distances.

Finally, in Fig. 6 we examine differences between nearby and more distant halo stars (also discussed by Xue et al. 2011). The left-hand panel corresponds to the full range of the Xue et al. (2008) sample ( $5 < r < 60$  kpc), the central panel corresponds to nearby stars ( $5 < r < 20$  kpc) which we excluded in Fig. 4 and the right-hand panel corresponds to the most distant stars in the sample ( $30 < r < 60$  kpc). As shown in Fig. 3, including nearby stars considerably reduces the amplitude of  $\xi(<\Delta)$  for MW halo BHBs, although the signal in the lowest bins remains significantly above zero. The observational data are dominated by stars at  $r < 20$  kpc and

hence the MW signal is essentially identical in the left and central panels.

In the whole-halo sample (left-hand panel of Fig. 6) some of the simulations (particularly Aq-A and Aq-B) show a reduction in  $\xi(<\Delta)$  on small scales, qualitatively similar to the observations. Nevertheless, Fig. 6 suggests that the contrast of structure against smoothly distributed stars is too high in our models, and that the discrepancy is most pronounced in the inner halo. Selecting an inner-halo sample (central panel of Fig. 6) emphasizes this point. The inner halo shows a similar degree of clustering in all six haloes, in all cases somewhat lower than the outer halo signal (on intermediate scales), but much stronger than the MW data. This panel reinforces our comments above on the structure of the haloes: Aq-C resembles Aq-A and Aq-D in the inner halo, because this distance range excludes the massive coherent streams that are the likely source of the strong signal seen in Fig. 4. Most of the coherent structure in Aq-E is nearby and the inclusion of stars at greater distances *diminishes* the average signal. This is in contradiction to the phase-mixing explanation for a more structured outer halo, but Aq-E is unusual in that for  $r < 20$  kpc it is dominated by a highly oblate, coherently rotating component (somewhat resembling a very thick disc, but with a significant radial velocity dispersion). Aq-B has a similar spherically averaged density profile to Aq-E, but here the inner halo shows less correlation, as expected. In Aq-F,  $\xi(<\Delta)$  is dominated by nearby stars, although these are highly clustered in phase space.

The comparison with more distant stars shown in the right-hand panel of Fig. 6 suggests that most of the models are consistent with the data in this region of the halo. Only Aq-C is clearly discrepant (Aq-D is marginally inconsistent at scales below  $\Delta \sim 12$  kpc). That our simulations more closely match the outer regions of the halo (beyond 30 kpc) support the view that these regions are dominated by stars accreted from satellites (Font et al. 2011; Xue et al. 2011). The outer stellar halo of the MW appears to be typical (or perhaps slightly more structured than average) with respect to our sample of six plausible realizations of dark matter haloes with similar mass.

## 7 CONCLUSIONS

We have analysed a correlation function for halo stars,  $\xi(<\Delta)$ , defining their separation in four dimensions of phase space using a

metric (which we call  $\Delta$ ) in readily obtained observables (angular and radial separation and radial velocity difference). A statistic of this type usefully quantifies kinematic and spatial substructure in the halo, and can be applied to observational data and catalogues generated from theoretical models. This analysis is particularly well suited to the distant halo – other methods for studying clustering in many dimensions may be more suitable for the ‘fine grained’ data on the nearby halo that will be obtained by the *Gaia* mission (e.g. Gómez et al. 2010).

We have measured  $\xi(<\Delta)$  for a large catalogue of spectroscopically confirmed BHB stars from SDSS (Xue et al. 2008). We find significant clustering in these data, particularly when we restrict the sample to stars with Galactocentric distance  $r > 20$  kpc. This finding of stronger phase-space correlations between stars in the outer halo is in agreement with that of Xue et al. (2011).

To test models of the accreted components of stellar haloes and understand the effects of sample variance, we have computed  $\xi(<\Delta)$  for mock observations constructed from the six  $\Lambda$ CDM simulations of Cooper et al. (2010) in which only the stellar haloes produced by disrupted satellites are considered. Our statistic distinguishes quantitatively between these six qualitatively different halo realizations. When only stars with  $r > 20$  kpc are considered, five of our six simulations show statistically significant correlations on scales in our metric equivalent to  $\sim 1\text{--}8$  kpc (for all observers on the solar circle). Most of the models are consistent with the MW data for the outer halo,  $r > 30$  kpc. For the inner halo, however, particularly at Galactocentric distances smaller than 20 kpc, the simulations tend to be significantly more strongly clustered than the data. One possible explanation for this is a deficiency of smoothly distributed halo stars in the models, perhaps attributable to the absence of so-called ‘*in situ*’ halo stars. These stars may be scattered from the Galactic disc, or born on eccentric orbits (in streams of accreted gas or an unstable cooling flow, for example). Neither of these processes is included in our model of the accreted halo.

Although it seems reasonable to expect that *in situ* haloes are distributed with spherical or axial symmetry and have a low degree of coherence in phase space, models of such components and predictions for the fraction of stars they contain are not well constrained. Most hypotheses for *in situ* halo formation limit these stars to an ‘inner’ halo and predict that the accreted component (which we simulate) dominates at larger radii (e.g. Abadi et al. 2006; Zolotov et al. 2009; Font et al. 2011). However, the fraction of the halo formed *in situ* and the boundary between ‘inner’ and ‘outer’ halo are highly model dependent. Detections of observable ‘dichotomies’ in the MW halo (Carollo et al. 2007) are still debated (e.g. Beers et al. 2011; Schönrich, Asplund & Casagrande 2011). It is possible to place broad limits on the fraction of stars in a ‘missing’ smooth component, for example by comparing the rms variation of projected star counts in our models (Helmi et al. 2011) to the MW (Bell et al. 2008). However, the uncertainties involved are substantial.

Another factor in the discrepancy between the models and the data may be the absence of a baryonic (disc) contribution to the gravitational potential. A massive disc could alter the process of satellite disruption in the inner halo and might make the potential within 30 kpc more spherical (Kazantzidis, Abadi & Navarro 2010), possibly distributing more inner halo stars into the SDSS footprint (on the other hand, a more axisymmetric or spherical dark halo might also result in fewer chaotic orbits, hence more coherent streams). Because of these modelling uncertainties, our application of the  $\xi(<\Delta)$  statistic can presently serve only as a basic test for the abundance of substructure in the simulations.

Several aspects of our approach could be improved. It seems desirable to use well-measured radial velocity data to enhance clustering signals such as our correlation function relative to those based on configuration space data alone. However, so far, no proposal for including these velocity data is well supported by theory. Here, we have used a straightforward choice of parametrized metric to illustrate the concept of scaling radial velocity separations to ‘equivalent’ configuration space separations, and this is empirically useful in recovering a measurable signal. Nevertheless, we have not found any compelling or generic way to select the scaling parameter ( $w_v$ ). Improving either the definition of the metric itself or the means of fixing this parameter is a clear priority for extensions of this approach. A similar issue affects the weighting of velocity information in clustering algorithms (e.g. Sharma et al. 2010).

Finally, further comparisons between stellar halo models and observational data should also account for the selection effects such as spectroscopic incompleteness and the potential bias of BHB stars as a tracer of the stellar halo (Bell et al. 2010; Xue et al. 2011). For statistical analysis, there is a pressing requirement for observational samples with well-understood selection functions, even if they do not probe the most distant halo. The LAMOST Galactic survey is likely to be the first to approach this goal.

In summary, we have taken a first step in adapting a well-studied cosmological statistic, the two-point correlation function, to the study of the MW halo. Our comparisons highlight the complexity of statistical analysis in the stellar halo, and the importance of interpreting observational results in the context of realistic models of halo assembly. We have compared the SDSS data with the stellar haloes produced by disrupted satellites in *ab initio* galaxy formation models constructed from the Aquarius  $N$ -body simulations of galactic dark haloes in the  $\Lambda$ CDM cosmology. With further refinements and more data, our statistical approach to quantifying the smoothness of the halo can provide a practical and productive way to study the structure of the MW halo and compare with theoretical expectations.

## ACKNOWLEDGMENTS

The authors thank Heather Morrison and the Spaghetti Survey team for making their data available prior to publication, and Xiangxiang Xue and Sergey Koposov for their assistance. We thank the referee for their helpful comments which greatly improved the structure of this paper. APC acknowledges an STFC studentship and thanks Else Starkenburg for useful discussions. SC acknowledges the support of a Leverhulme Research Fellowship. CSF acknowledges a Royal Society Wolfson Research Merit Award and ERC Advanced Investigator grant 267291-COSMIWAY. AH acknowledges funding support from the European Research Council under ERC-StG grant GALACTICA-24027. This work was supported in part by an STFC rolling grant to the ICC. The calculations for this paper were performed on the ICC Cosmology Machine, which is part of the DiRAC Facility jointly funded by STFC, the Large Facilities Capital Fund of BIS and Durham University. Fig. 1 was produced with the HEALPY implementation of HEALPIX (<http://healpix.jpl.nasa.gov/>; Gorski et al. 2005).

## REFERENCES

- Abadi M. G., Navarro J. F., Steinmetz M., 2006, MNRAS, 365, 747
- Abadi M. G., Navarro J. F., Fardal M., Babul A., Steinmetz M., 2010, MNRAS, 407, 435
- Beers T. C. et al., 2011, preprint (arXiv:1104.2513)

- Bell E. F. et al., 2008, *ApJ*, 680, 295  
 Bell E. F., Xue X. X., Rix H. W., Ruhland C., Hogg D. W., 2010, *ApJ*, 140, 1850  
 Bower R. G., Benson A. J., Malbon R., Helly J. C., Frenk C. S., Baugh C. M., Cole S., Lacey C. G., 2006, *MNRAS*, 370, 645  
 Brown W. R., Geller M. J., Kenyon S. J., Beers T. C., Kurtz M. J., Roll J. B., 2004, *AJ*, 127, 1555  
 Brown A. G. A., Velázquez H. M., Aguilar L. A., 2005, *MNRAS*, 359, 1287  
 Bullock J. S., Johnston K. V., 2005, *ApJ*, 635, 931  
 Carollo D. et al., 2007, *Nat*, 450, 1020  
 Cooper A. P. et al., 2010, *MNRAS*, 406, 744  
 Dehnen W., Binney J. J., 1998, *MNRAS*, 298, 387  
 De Lucia G., Helmi A., 2008, *MNRAS*, 391, 14  
 Dohm-Palmer R. C., Mateo M., Olszewski E., Morrison H., Harding P., Freeman K. C., Norris J., 2000, *AJ*, 120, 2496  
 Doinidis S. P., Beers T. C., 1989, *ApJ*, 340, 57  
 Font A. S., McCarthy I. G., Crain R. A., Theuns T., Schaye J., Wiersma R. P. C., Dalla Vecchia C., 2011, *MNRAS*, in press (doi:10.1111/j.1365-2966.2011.19227.x) (arXiv:1102.2526)  
 Freeman K., Bland-Hawthorn J., 2002, *ARA&A*, 40, 487  
 Gómez F. A., Helmi A., 2010, *MNRAS*, 401, 2285  
 Gómez F. A., Helmi A., Brown A. G. A., Li Y. S., 2010, *MNRAS*, 408, 935  
 Górski K. M., Hivon E., Banday A. J., Wandelt B. D., Hansen F. K., Reinecke M., Bartelmann M., 2005, *ApJ*, 622, 759  
 Gould A., 2003, *ApJ*, 592, 63  
 Helmi A., de Zeeuw P. T., 2000, *MNRAS*, 319, 657  
 Helmi A., Cooper A. P., White S. D. M., Cole S., Frenk C. S., Navarro J. F., 2011, *ApJ*, 733, L7  
 Johnston K. V., Bullock J. S., Sharma S., Font A., Robertson B. E., Leitner S. N., 2008, *ApJ*, 689, 936  
 Kazantzidis S., Abadi M. G., Navarro J. F., 2010, *ApJ*, 720  
 Lemon D. J., Wyse R. F. G., Liske J., Driver S. P., Horne K., 2004, *MNRAS*, 347, 1043  
 Libeskind N. I., Frenk C. S., Cole S., Helly J. C., Jenkins A., Navarro J. F., Power C., 2005, *MNRAS*, 363, 146, 62  
 Lovell M. R., Eke V. R., Frenk C. S., Jenkins A., 2011, *MNRAS*, 413, 3013  
 Maciejewski M., Colombi S., Alard C., Bouchet F., Pichon C., 2009, *MNRAS*, 393, 703  
 Morrison H. L., Mateo M., Olszewski E. W., Harding P., Dohm-Palmer R. C., Freeman K. C., Norris J. E., Morita M., 2000, *AJ*, 119, 2254  
 Re Fiorentin P., Helmi A., Lattanzi M. G., Spagna A., 2005, *A&A*, 439, 551  
 Schlaufman K. C. et al., 2009, *ApJ*, 703, 2177  
 Schönrich R., Asplund M., Casagrande L., 2011, *MNRAS*, 415, 3807  
 Searle L., Zinn R., 1978, *ApJ*, 225, 357  
 Sharma S., Johnston K. V., 2009, *ApJ*, 703, 1061  
 Sharma S., Johnston K. V., Majewski S. R., Muñoz R. R., Carlberg J. K., Bullock J., 2010, *ApJ*, 722, 570  
 Springel V. et al., 2008, *MNRAS*, 391, 1685  
 Starkenburg E. et al., 2009, *ApJ*, 698, 567  
 Tissera P. B., White S. D. M., Pedrosa S., Scannapieco C., 2010, *MNRAS*, 406, 922  
 Vera-Ciro C. A., Sales L. V., Helmi A., Frenk C. S., Navarro J. F., Springel V., Vogelsberger M., White S. D. M., 2011, *MNRAS*, 416, 1377  
 Walker M. G., Mateo M., Olszewski E. W., Peñarrubia J., Wyn Evans N., Gilmore G., 2009, *ApJ*, 704, 1274  
 Wang J. et al., 2011, *MNRAS*, 413, 1373  
 White S. D. M., Springel V., 2000, in Weiss A., Abel T. G., Hill V., eds, *The First Stars*. Springer, Berlin, p. 327  
 Xue X. X. et al., 2008, *ApJ*, 684, 1143  
 Xue X. X., Rix H. W., Zhao G., 2009, *Res. Astron. Astrophys.*, 9, 1230  
 Xue X. X. et al., 2011, *ApJ*, 738, 79  
 Zolotov A., Willman B., Brooks A. M., Governato F., Brook C. B., Hogg D. W., Quinn T., Stinson G., 2009, *ApJ*, 702, 1058

This paper has been typeset from a Te<sub>X</sub>/La<sub>T</sub>e<sub>X</sub> file prepared by the author.